Supplementary materials for

High breakdown strength and energy storage performance in (Nb, Zn) modified $SrTiO_3$ ceramics via synergy manipulation

Wengao Pan [a], Minghe Cao [a]*, Abdullah Jan [a], Hua Hao [a], Zhonghua Yao [a], Hanxing Liu [b]

[a] State Key Laboratory of Advanced Technology for Materials Synthesis and Processing, Wuhan University of Technology, Wuhan, 430070, PR China

[b] International School of Materials Science and Engineering, Wuhan University of Technology, Wuhan, 430070, PR China

*Corresponding Author: E-mail: caominghe@whut.edu.cn

The Supplementary Materials include:

- Finite element simulation method.
- Fig. S1, Fig. S2, Fig. S3 and Fig. S4.
- Table S1 and Table S2.
- The corresponding references.

Finite element simulation method

Firstly, Grain model was elaborately built referring to the real grain size and impurity amount by Voronoi tessellation using 3D modeling software. To ensure the corresponding relation between the model and sample, the mass fraction of 4.5 wt% is converted into volume fraction, and then make sure the area ratio between grain boundary region and the grain region is approximately equal to the volume fraction.

Secondly, the electrical parameters of $SrTi_{0.985}Nb_{0.01}Zn_{0.005}O_3$ (STZN) ceramics and $ZnNb_2O_6$ (ZN) additives were confirmed by a precision impedance analyzer (E4980A; Agilent Tech) and a pA electrometer (6517A, Keithley, USA), respectively. The permittivity of STZN and ZN are 1700 and 25, separately. The conductivity of STZN and ZN are 1.1×10^{-9} S/cm and 2.5×10^{-12} S/cm, respectively.

Thirdly, separately assign these parameters to grain and grain boundary regions in COMSOL Multiphysics software, and then begin the finite element simulation under the critical electric field intensity.

Figures

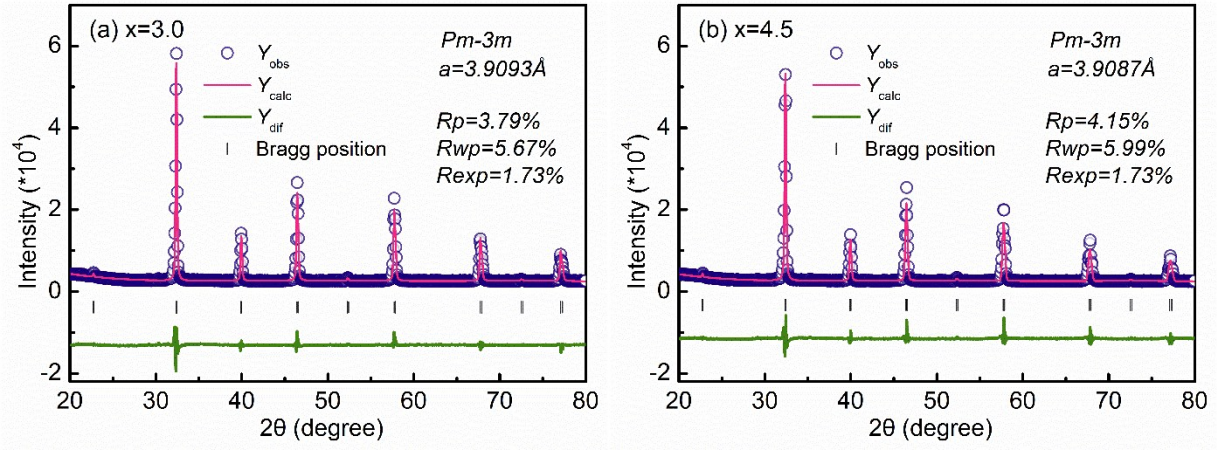

Fig. S1. XRD refinement results of x=3.0 (a) and x=4.5 (b) ceramics

Fig. S1(a) and (b) are the XRD refinement results of x=3.0 and x=4.5 ceramics, both the two

ceramics can be well refined by Pm-3m space group, indicating that no obvious phase transition can be expected.

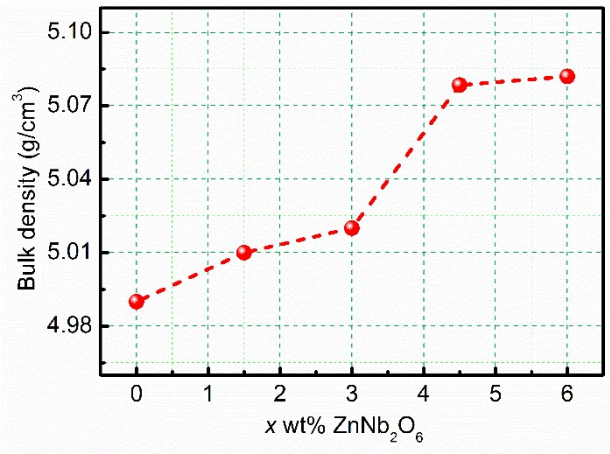

Fig. S2. Bulk density of the ceramics with different content of $ZnNb_2O_6$ additives

Fig. S2 is the bulk density of the ceramics measured by Archimedes method. It can be seen that with the increase content of $ZnNb_2O_6$ additives, the bulk density gradually increases and finally tend to be stable at a higher addition amount.

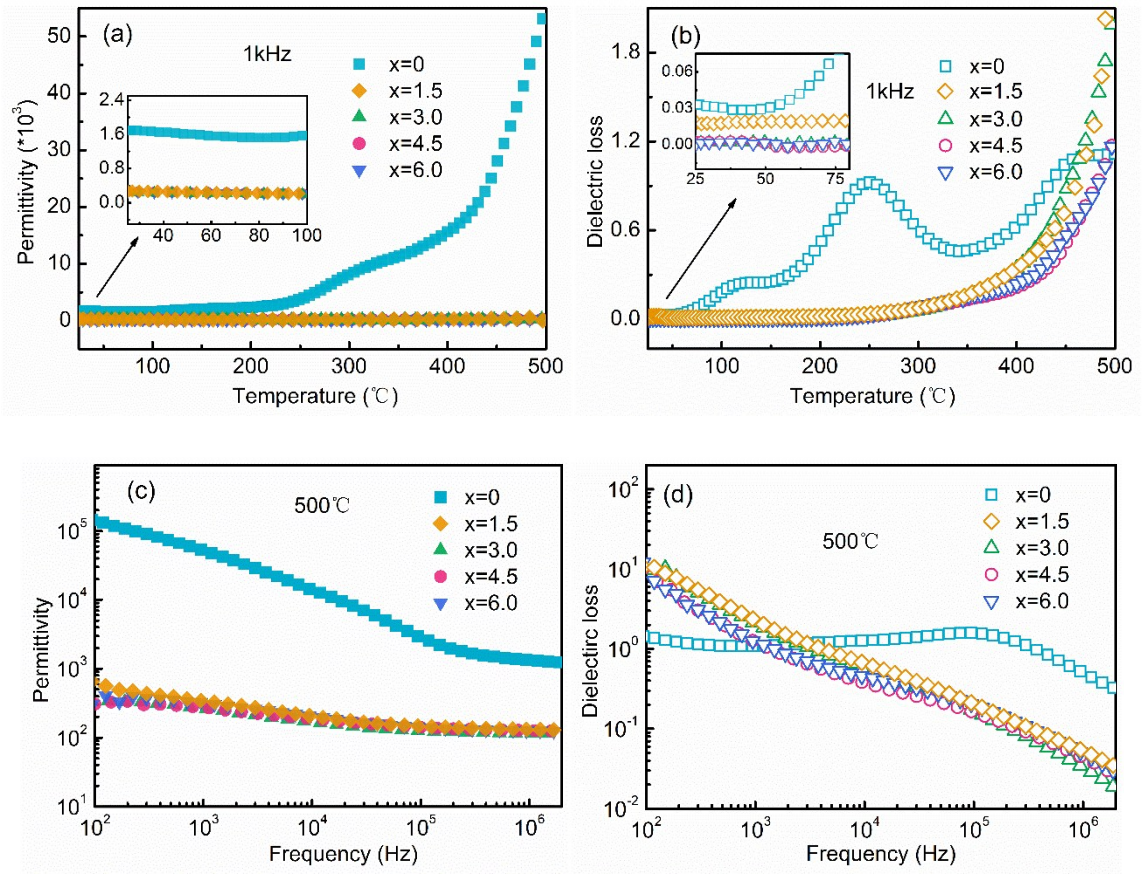

Fig. S3. Temperature (a-b) and frequency (c-d) dependent dielectric properties of the STZN-x wt%ZN ceramics

Fig. S3 (a-b) are the temperature dependent dielectric properties measured at 1kHz. Compared with the pure STZN ceramics, ZN doped STZN ceramics become extreme stability in permittivity and dielectric loss relaxation peaks are also significantly suppressed. Fig. S3 (c-d) present the frequency dependent dielectric properties measured at 500 °C. Permittivity of ZN doped STZN ceramics exhibit excellent stability in a wide frequency range (20-2 MHz) and the dielectric loss decline gradually with increase of the frequency.

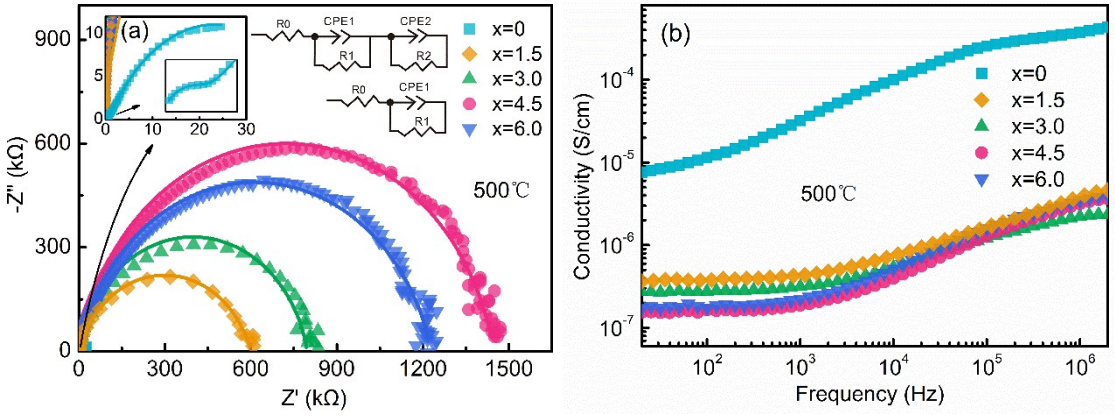

Fig. S4. (a) Complex impedance spectroscopy measured at 500 °C. Inserts are the equivalent circuits and local magnification. (b) Frequency dependence of conductivity measured at 500 °C.

To further understand the electrical properties of ceramics, complex impedance spectroscopies of the ceramics are measured at 500 °C, as shown in Fig. S4 (a). The inserts present the local enlarged view and equivalent circuits. Pure STZN ceramics exhibit two semicircles while four STZN-ZN ceramics display only one semicircle in the whole measured frequency range, indicating that the difference between grain and grain boundary tends to be vague due to introduction of ZN. Insulativity of samples can be roughly evaluated by comparing the semicircle radius of them. Then, semicircle radius of ceramics x=4.5 is larger than those of others indicates the higher insulation resistances. Fig. S4 (b) shows the frequency dependence of conductivity measured at 500 °C. With increase of

frequency, conductivities of all the ceramics increase gradually. Compared with other samples, the x=4.5 ceramics exhibits a lower conductivity, further confirming the excellent insulation properties.

Tables

Table S1 The polarization and energy storage properties under critical electric field

	E_{max} (kV/cm)	P_{max} (μC/cm^2)	P_r (μC/cm^2)	ΔP (μC/cm^2)	W_c (J/cm^3)	W_d (J/cm^3)	η (%)
x=1.5	285	6.75	0.54	6.21	1.03	0.83	80.6
x=3.0	295	7.05	0.84	6.21	1.13	0.84	74.3
x=4.5	422	10.44	1.10	9.34	2.35	1.81	77.0
x=6.0	389	9.27	0.95	9.32	1.93	1.50	77.7

Table S2 Energy storage property comparisons between this work and related ceramic dielectrics

Material systems	E_b (kV/cm)	W_c (J/cm^3)	η (%)
$0.9CaTiO_3$-$0.1BiScO_3$ [1]	270	1.71	90.4
$0.91BaTiO_3$-$0.09BiYbO_3$ [2]	93	0.67	82.6
$Ba_{0.4}Sr_{0.6}TiO_3$ with Bi_2O_3-B_2O_3-SiO_2 [3]	279	2.19	90.57
$BaTiO_3$-$Bi_{0.5}Na_{0.5}TiO_3$-$Na_{0.73}Bi_{0.09}NbO_3$ [4]	172	2.07	82
$BaTiO_3$@$SrTiO_3$ [5]	47	0.24	90
$BiFeO_3$-$BaTiO_3$-$Ba(Mg_{1/3}Nb_{2/3})O_3$ [6]	125	2.08	75
$BiFeO_3$- $BaTiO_3$-$La(Mg_{1/2}Ti_{1/2})O_3$ [7]	130	1.66	82
$BaTiO_3$/$BaTiO_3$@SiO_2 [8]	301	1.80	74
$Ba_{0.4}Sr_{0.6}TiO_3$ with SiO_2 [9]	134	1.09	79
$Sr_{0.985}Ce_{0.01}TiO_3$@SiO_2 [10]	290	2.24	50
$0.85BaTiO_3$-$0.15Bi(Mg_{1/2}Zr_{1/2})O_3$ [11]	185	1.25	95
$Ba_{0.3}Sr_{0.7}TiO_3$@ SiO_2 [12]	380	1.85	82
$SrSn_{0.05}Ti_{0.95}O_3$ [13]	255	1.10	87
$SrTiO_3$@SiO_2 [14]	310	1.58	76

$BaTiO_3$-$Bi_{0.5}Na_{0.5}TiO_3$-$SrY_{0.5}Nb_{0.5}O_3$ [15]	152	1.83	74.3
$0.88BaTiO_3$-$0.12Bi(Li_{0.5}Nb_{0.5})O_3$ [16]	270	2.31	88
$Ba_{0.4}Sr_{0.6}TiO_3$-MgO [17]	300	1.69	88.5
$Sr_{0.7}Ba_{0.3}Nb_2O_6$-MgO [18]	157	1.04	89.4
$SrTiO_3$-$Bi_{0.54}Na_{0.46}TiO_3$-$BaTiO_3$ [19]	177	2.38	79
$0.90(Na_{0.5}Bi_{0.5})TiO_3$-$0.10KNbO_3$ [20]	104	1.42	82.3
This work	422	2.35	77

References

[1] B. C. Luo, X. H. Wang, E. K. Tian, H. Z. Song, H. X. Wang, L.T. Li , *ACS Appl. Mater. Interfaces*, 2017, **9**, 19963−19972.

[2] Z. B. Shen, X. H. Wang, B. C. Luo, L. T. Li, *J. Mater. Chem. A*, 2015, **3**, 18146-18153.

[3] H. B. Yang, F. Yan, Y. Lin, T. Wang, *J. Eur. Ceram. Soc.*, 2018, **38**, 1367-1373.

[4] H. B. Yang, F. Yan, Y. Lin, T. Wang, F. Wang, Y. L. Wang, L. N. Guo, W. D. Tai, H. Wei, *J. Eur. Ceram. Soc.*, 2017, **37**, 3303-3311.

[5] L. W. Wu, X. H. Wang, H. L. Gong, Y. N. Hao, Z. B. Shen, L. T. Li, *J. Mater. Chem. C*, 2015, **3**, 750-758.

[6] D. Zheng, R. Zuo, D. Zhang, Y. Li, *J. Am. Ceram. Soc.*, 2015, **98**, 2692-2695.

[7] D. G. Zheng, R. Z. Zuo, *J. Eur. Ceram. Soc.*, 2017, **37**, 413-418.

[8] Q. B. Yuan, J. Cui, Y. F. Wang, R. Ma, H. Wang, *J. Eur. Ceram. Soc.*, 2017, **37**, 4645-4652.

[9] C. L. Diao, H. X. Liu, H. Hao, M. H. Cao, Z. H. Yao, *Ceram. Int.*, 2016, **42**, 12639-12643.

[10] J. L. Qi, M. H. Cao, J. P. Heath, J. S. Dean, H. Hao, Z. H. Yao, Z. Y. Yu, H. X. Liu, *J. Mater. Chem. C*, 2018, **6**, 9130-9139.

[11] X. W. Jiang, H. Hao, S. J. Zhang, J. H. Lv, M. H. Cao, Z. H. Yao, H. X. Liu, *J. Eur. Ceram. Soc.*,

2019, **39**, 1103-1109.

[12] M. Liu, M. H. Cao, F. Z. Zeng, J. L. Qi, H. X. Liu, H. Hao, Z. H. Yao, *Ceram. Int.*, 2018, **44**, 20239-20244.

[13] J. Xie, H. Hao, H. X. Liu, Z. H. Yao, Z. Song, L. Zhang, Q. Xu, J. Q. Dai, M. H. Cao, *Ceram. Int.*, 2016, **42**, 12796-12801.

[14] F. Z. Zeng, M. H. Cao, L. Zhang, M. Liu, H. Hao, Z. H. Yao, H. X. Liu, *Ceram. Int.*, 2017, **43**, 7710-7716.

[15] X. Y. Liu, H. B. Yang, F. Yan, Y. Qin, Y. Lin, T. Wang, *J. Alloys Compd.*, 2019, **778**, 97-104.

[16] W. B. Li, D. Zhou, L. X. Pang, R. Xu, H. H. Guo, *J. Mater. Chem. A*, 2017, **5**, 19607-19612.

[17] Y. H. Huang, Y. J. Wu, W. J. Qiu, J. Li, X. M. Chen, *J. Eur. Ceram. Soc.*, 2015, **35**, 1469-1476.

[18] Y. Rao, H. X. Liu, H. Hao, Z. H. Yao, X. X. Zhou, M. H. Cao, Z. Y. Yu, *Ceram. Int.*, 2018, **44**, 11022-11029.

[19] C. Wang, F. Yan, H. B. Yang, Y. Lin, T. Wang, *J. Alloys Compd.*, 2018, **749**, 605-611.

[20] L. Luo, B. Wang, X. Jiang, W. Li, *J. Mater. Sci.*, 2014, **49**, 1659-1665.